1.1+-0.66 mm (3D) interfractionally. The 3D RMS estimation of error correlated significantly with the distance between the two markers ($p<0.001$), with an R^2 of 0.59 for intrafraction errors, see Fig. 1. Different motion trajectories of the markers due to breathing, was the main cause of intrafraction errors. As the interfraction error estimate was based on average positions during CBCT acquisition, the effects of breathing were be less pronounced, and errors were most likely caused by drift of markers, liver deformations, and variations in patient rotation.

Conclusions: We have quantified the intra- and inter-fraction prediction error of liver fiducial markers. In general, during treatment, the position of a marker could be predicted with a 3D RMS error below 1.5 mm from another surrogate marker when the distance between the markers were less than 5 cm. Between fractions, there was an average 3D RMS error of 1.1 +-0.66 mm.

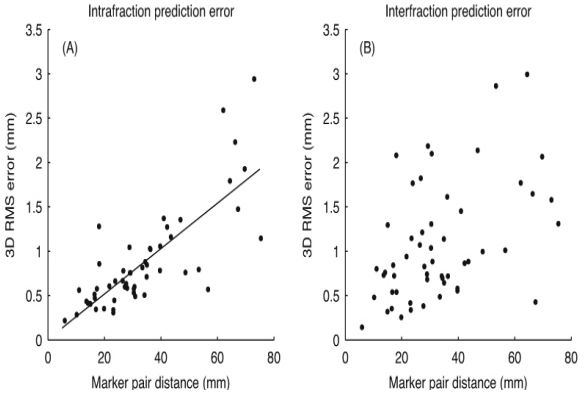

OC-0337

Assessment of fast external and internal motion surrogates to supplement MRI based tracking of the pancreas

B. Stemkens[1], R.H. Tijssen[1], B. Denis de Senneville[2], J.J.W. Lagendijk[1], C.A.T. van den Berg[1]
[1]*UMC Utrecht, Radiotherapy, Utrecht, The Netherlands*
[2]*UMC Utrecht, Image Science Institute, Utrecht, The Netherlands*

Purpose/Objective: Radiotherapy for pancreatic tumors is currently limited by respiratory induced motion. Precise motion management is vital to ensure full dose coverage and limit toxicity in nearby organs at risk (OAR). MR-guidance opens up the way to visualize tumors and track OARs during treatment (Lagendijk, 2008). Volumetric (3D) MR-imaging, however, is currently not fast enough to achieve the temporal resolution required for real-time beam steering. We therefore investigate two (fast) surrogate motion markers for pancreatic motion to be used in conjunction with (slower) 3D MRI. External monitoring by means of a respiratory pressure belt, is compared to internal tracking based on the motion of the diaphragm.

Materials and Methods: 2D radial cine MR scans (bSSFP; TE/TR = 1.29ms/2.6 ms) were acquired in six healthy subjects during free-breathing (2m50s, 3 frames/sec). Scan planes were angulated parallel to the principal axis of motion. Simultaneously, the breathing signal was recorded using a respiratory pressure belt (surrogate 1). 1D MR navigators were simulated by tracking the cranial-caudal (CC) diaphragm motion on the 2D scans.

Image analysis: Pancreatic motion is estimated on MR images, as reference data, using the optical flow algorithm, which has been successfully applied and validated for HIFU treatments (Roujol, 2011). The diaphragm motion (surrogate 2) was assessed separate from the pancreas motion. Power spectrum analysis were used to give insight in the CC motion frequencies. To assess the agreement of the surrogate motion markers and pancreatic motion, a general linear model (GLM) was calculated using $Y = \beta X + \varepsilon$, in which Y is the pancreatic motion, β the parameter estimate, X the surrogate motion signal (diaphragm or belt), and ε represents the residual error. Z-statistics are calculated to determine the model conformity.

Results: All power spectra show peaks at the principle respiratory frequency (**Fig 1a**). However, significant low frequent components can be seen in the power spectra of the 2D cine-MRI and the navigator, whereas the respiratory belt shows only one small peak. Visual inspection of the data showed a global rigid body movement of the subject, which can not be detected by the belt. Both models showed good z-statistics for the pancreas. However, the residual error in the pancreas is much lower for the diaphragm surrogate (**Fig. 1b** and **c**). This implies that the diaphragm moves rigidly in a CC direction with the liver and pancreas and is thus a better predictor for motion than the respiratory belt. As expected, both models showed high residual error for through-plane motion (e.g. intestines).

Conclusions: This data shows that diaphragm tracking (which can be accomplished with fast 1D MR navigators) is a better surrogate for pancreatic motion than external monitoring using a respiratory pressure belt. Furthermore, left-right motion can be characterized (results not shown) using internal tracking, which is not possible using external monitoring. Therefore, external monitoring should be used with care in motion characterization and prediction models.

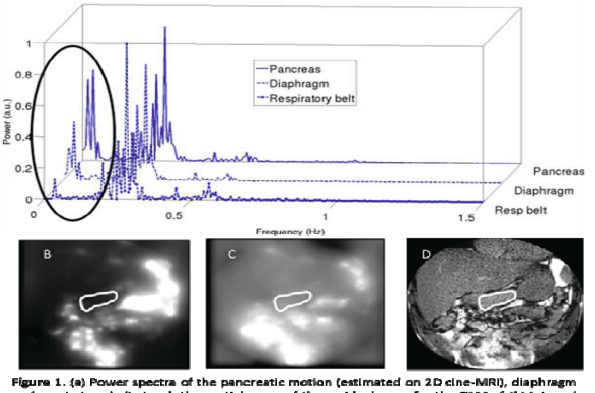

Figure 1. (a) Power spectra of the pancreatic motion (estimated on 2D cine-MRI), diaphragm and respiratory belt signal, the spatial maps of the residual error for the GLM of (b) internal tracking (1D MR navigator) and (c) external monitoring (respiratory belt) and (d) an anatomical reference image with the pancreas encircled.

OC-0338

Accuracy of a predictive model in IR-marker-based dynamic tumour tracking for lung cancer

M. Akimoto[1], M. Nakamura[1], N. Mukumoto[1], H. Tanabe[2], M. Yamada[1], Y. Matsuo[1], H. Monzen[1], T. Mizowaki[1], M. Kokubo[3], M. Hiraoka[1]
[1]*Kyoto University Graduate School of Medicine, Department of Radiation Oncology and Image-applied Therapy, Kyoto, Japan*
[2]*Institute of Biomedical Research and Innovation, Division of Radiation Oncology, Kobe, Japan*
[3]*Kobe City Medical Center General Hospital, Department of Radiation Oncology, Kobe, Japan*

Purpose/Objective: We have applied infrared (IR)-marker-based dynamic tumour tracking irradiation (IR tracking) with Vero4DRT (MHI-TM2000) clinically to lung cancer patients since September 2011. This study quantified the accuracy of the predictive model of IR tracking for lung cancer using log files.

Materials and Methods: Before beam delivery, a predictive model (4D model), which correlates the displacement of IR markers on the abdomen with the three-dimensional (3D) position of a tumour indicated by implanted gold markers, is required. The IR and gold markers were monitored for 40 s with the IR camera every 16.7 ms and an orthogonal kV X-ray imaging subsystem every 80 or 160 ms, respectively. The 4D model predicted the future target position from the displacement of the IR markers in real-time, and the gimbaled x-ray head then tracked the moving tumour continuously, based on the predicted target position. In clinical practice, we updated the 4D model at least once during each treatment session to ensure predictive accuracy.

This study evaluated the 4D modelling error (E_{4DM}) and influence of the intrafractional baseline drift of the IR marker position on the predicted target position (E_{IR}). E_{4DM} was defined as the difference between the predicted and detected target positions during the modelling duration and E_{IR} was defined as the difference between the predicted target positions generated from parameters of previous and updated 4D model. For E_{4DM} and E_{IR}, the overall mean (M), systematic (Σ), and random (σ) errors were calculated from the log files of ten patients who underwent IR tracking. A total of 112 and 55 log files were analyzed for the E_{4DM} and E_{IR}, respectively.

Results: The respiratory motion amplitudes of the lung tumours ranged from 1.0–7.5, 4.7–28.5, and 2.4–10.5 mm in the left-right (LR), cranio-caudal (CC), and anterior-posterior (AP) directions, respectively. For the E_{4DM}, (M, Σ, σ) (in mm) were (0.0, 0.0, 0.4), (0.0, 0.0, 0.8), and (0.0, 0.0, 0.6) in the LR, CC, and AP directions, respectively. The local maximum E_{4DM} commonly appeared around the peak of the respiratory pattern (Fig. 1). The median time elapsed until the 4D model was updated was 13 (range 2–23) min. For the E_{IR}, (M, Σ, σ) (in mm) were (0.0, 0.3, 0.2), (0.2, 0.9, 0.5), and (0.4, 0.6, 0.3) in the LR, CC, and AP directions, respectively. If the 4D model was not updated in the presence of intrafractional baseline drift, the predicted target position deviated from the detected target position systematically (Fig. 1).

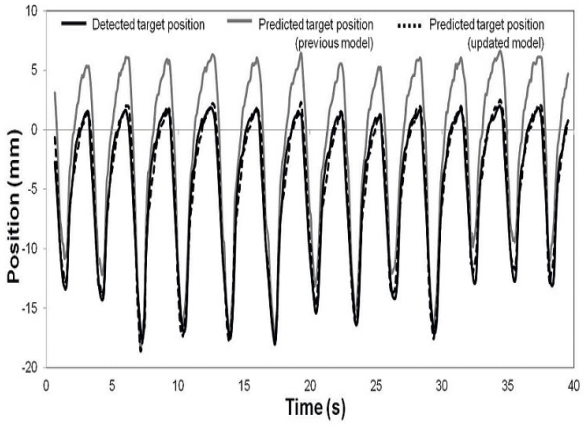

Figure 1. The detected target position and the predicted target positions based on the previous and updated 4D models in the CC direction.

Conclusions: The log file analyses of real clinical cases showed that the intrafractional baseline drift was not negligible, although the geometric error caused by respiratory motion was reduced substantially by applying IR tracking; therefore, it is necessary to check constantly IR marker position and update the 4D model several times during a treatment session.

PROFFERED PAPERS: PHYSICS 8: PROTON TREATMENT PLANNING AND PLAN COMPARISON

OC-0339

Improving IMPT treatment planning using iterative resampling of randomly placed pencil beams

S. Van de Water[1], A.C. Kraan[1], S. Breedveld[1], W. Schillemans[1], D.N. Teguh[1], H.M. Kooy[2], T.M. Madden[2], B.J.M. Heijmen[1], M.S. Hoogeman[1]
[1]*Erasmus MC - Daniel den Hoed Cancer Center, Radiation Oncology, Rotterdam, The Netherlands*
[2]*Massachusetts General Hospital and Harvard Medical School, Radiation Oncology, Boston MA, USA*

Purpose/Objective: In treatment planning for spot-scanned intensity modulated proton therapy (IMPT), candidate proton pencil beams are traditionally distributed over the target volume using a regular grid for each beam direction. The use of a coarse grid minimizes optimization times, but might result in compromised plan quality. Conversely, the use of a very fine grid might lead to excessive optimization times, especially for large target volumes. To improve the efficiency of multi-criteria IMPT treatment planning, we have developed an optimization method called 'pencil beam resampling'. The aim of this study is to investigate whether pencil beam resampling reduces optimization times and improves treatment plan quality for multi-criteria IMPT optimization.
Materials and Methods: Pencil beam resampling consists of repeated inverse multi-criteria optimization, while performing in each iteration: 1) random selection of new candidate pencil beams from a very fine grid and 2) reduction of the number of pencil beams in the present solution. Pencil beam resampling was implemented, next to regular grid planning, into our in-house developed treatment planning system 'iCycle'. The system optimizes objectives successively according to their priorities as defined in the so-called 'wish-list'. For five head-and-neck cancer patients and two pencil beam widths (3 mm and 6 mm sigma), treatment plans were generated for both optimization techniques. Pencil beam resampling was performed for 15 iterations using sample sizes of 1000, 3000 and 5000 randomly selected pencil beams per iteration. Regular grid plans were generated using a grid spacing ranging from 4x4x4 to 7x7x7 mm. Differences in optimization time (for comparable plan quality) and in plan quality parameters (for comparable optimization time) were assessed. Next to that, treatment plan robustness was compared by simulating setup errors of 5 mm in all directions and range errors of ± 3.5%.
Results: Pencil beam resampling resulted in an optimization time reduction of 69% on average, with a maximum of 94%, compared with the use of traditional regular grids. The optimization times are depicted in Figure 1. Doses to organs-at-risk were generally reduced when using pencil beam resampling instead of regular grid planning, with median dose reductions ranging from -0.3 to 2.6 Gy, depending on the organ. Maximum dose improvements ranged from 0.9 to 11.4 Gy. Thin and wide pencil beams displayed similar behavior in terms of optimization time reductions and plan quality improvements, although shorter optimization times and better plan quality were achieved using thin pencil beams. No significant effect of the optimization technique on the robustness against setup and range errors was observed.

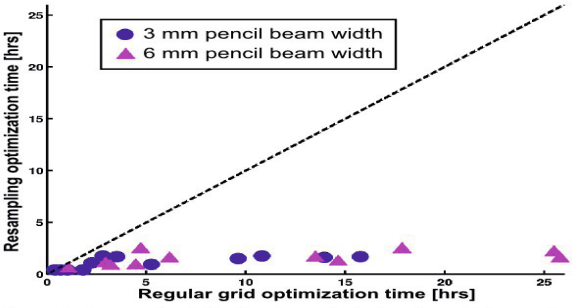

Figure 1. Scatter plot indicating the optimization time of the regular grid plans (horizontal axis) and the optimization time of the corresponding pencil beam resampling plans (vertical axis) with a comparable plan quality. Circles indicate plans generated with the thin pencil beam, triangles indicate results for the wide pencil beam.

Conclusions: Pencil beam resampling resulted in plan quality improvements and in considerable optimization time reductions compared with traditional regular grid planning.

OC-0340

Reproducibility of target coverage in stereotactic proton lung irradiation under high frequency jet ventilation

A. Santiago[1], U. Jelen[1], F. Ammazzalorso[1], R. Engenhart-Cabilic[1], P. Fritz[2], W. Mühlnickel[2], W. Enghardt[3], M. Baumann[3], A. Wittig[1]
[1]*University of Marburg, Department of Radiotherapy and Radiation Oncology, Marburg, Germany*
[2]*St Marien-Krankenhaus, Department of Radiotherapy, Siegen, Germany*
[3]*Medical Faculty and University Hospital Carl Gustav Carus Technische Universität Dresden, Department of Radiation Oncology and OncoRay - National Center for Radiation Research in Oncology, Dresden, Germany*

Purpose/Objective: To determine the changes in the planned PTV and GTV coverage between the treatment plan and the recomputation on the localization CT, for stereotactic proton irradiation in the lung under high frequency jet ventilation (HFJV).
Materials and Methods: Data sets of twelve patients treated for thirteen peripheral non-small cell lung cancer (NSCLC) tumors or solitary metastases with single-fractionated stereotactic photon therapy up to 33 Gy under HFJV were selected for this study. HFJV is a technique originally used for surgical procedures on the respiratory tract, which induces respiratory standstill, thus helping to reduce the GTV to PTV margins. HFJV might also allow a margin-based approach to motion management in lung particle therapy. All patients in the study received a planning CT and a localization CT, also under HFJV, in order to check the reproducibility of the tumor position shortly before the irradiation. Both CT scans and structures were imported into Pinnacle[3] TPS (version 8.0; Philips Radiation Oncology System, The Netherlands) where 6D patient bony anatomy registrations were performed on both data sets, and the structures from the planning CT were co-registered accordingly. For this study, only translational 3D corrections were introduced in the plan recalculation. Proton plans were created on the planning CT with TRiP98 TPS, a dedicated treatment planning system for scanning beam particle therapy, and recomputed on the localization CT (see picture below). The planning technique consisted of two coplanar beams entering the patient laterally at 0° and 45°, and the PTV was equal to the GTV plus 5 mm isotropic margin. Total dose was 33 Gy, aiming at 98% of the PTV receiving at least 95% of the prescribed dose (V95 equal to 98%). Dosimetric parameters were compared between the original and the recomputed plans and statistical significance was measured with Wilcoxon paired tests.